Neurotherapeutics 21 (2024) e00353

Contents lists available at ScienceDirect

Neurotherapeutics

journal homepage: www.sciencedirect.com/journal/neurotherapeutics

Original Article

Regulating Lars2 in mitochondria: A potential Alzheimer's therapy by inhibiting tau phosphorylation

Wenqi Qian [a,b,1], Lin Yuan [c,1], Weishan Zhuge [b,1], Liuqing Gu [a,b], Yutian Chen [b], Qichuan Zhuge [a,b,*], Haoqi Ni [a,b,*], Xinhuang Lv [a,b,*]

[a] Department of Neurosurgery, The First Affiliated Hospital of Wenzhou Medical University, Wenzhou, 325000, Zhejiang, China
[b] Zhejiang Provincial Key Laboratory of Aging and Neurological Disorder Research, The First Affiliated Hospital of Wenzhou Medical University, Wenzhou, 325000, Zhejiang, China
[c] Institute of Biomedical Sciences, Peking University Shenzhen Hospital, Shenzhen, 518036, China

ARTICLE INFO

Keywords:
Leucyl-tRNA synthetase 2
Mitochondrion
PI3K/AKT/GSK3β axis
Alzheimer's disease (AD)

ABSTRACT

Driven by the scarcity of effective treatment options in clinical settings, the present study aimed to identify a new potential target for Alzheimer's disease (AD) treatment. We focused on Lars2, an enzyme synthesizing mitochondrial leucyl-tRNA, and its role in maintaining mitochondrial function. Bioinformatics analysis of human brain transcriptome data revealed downregulation of Lars2 in AD patients compared to healthy controls. During *in vitro* experiments, the knockdown of Lars2 in mouse neuroblastoma cells (neuro-2a cells) and primary cortical neurons led to morphological changes and decreased density in mouse hippocampal neurons. To explore the underlying mechanisms, we investigated how downregulated Lars2 expression could impede the phosphatidylinositol 3-kinase/protein kinase B (PI3K-AKT) pathway, thereby mitigating AKT's inhibitory effect on glycogen synthase kinase 3 beta (GSK3β). This led to the activation of GSK3β, causing excessive phosphorylation of Tau protein and subsequent neuronal degeneration. During *in vivo* experiments, knockout of lars2 in hippocampal neurons confirmed cognitive impairment through the Barnes maze test, the novel object recognition test, and nest-building experiments. Additionally, immunofluorescence assays indicated an increase in p-tau, atrophy in the hippocampal region, and a decrease in neurons following Lars2 knockout. Taken together, our findings indicate that Lars2 represents a promising therapeutic target for AD.

Introduction

Alzheimer's disease (AD), a significant form of dementia, has raised global health concerns [1]. Characterized by memory deficit, cognitive decline, and behavior change, AD is considered a progressive neurodegenerative disease [2]. Its pathology involves the formation of amyloid-beta (Aβ) and hyperphosphorylated tau protein (p-tau) [3,4]. While previous studies focused on targeting Aβ pathology for potential AD therapy, clinical evidence suggests limited effectiveness in slowing disease progression. Accumulating evidence suggests that abnormal tau phosphorylation, rather than Aβ, is more closely related to cognitive impairment. Consequently, significant interest lies in tau protein-targeted treatments as a potential therapeutic approach for AD [5–7]. Abundant in axons and expressed in neurons, tau regulates processes like vesicular transport and axonal trafficking [7–9]. Tau phosphorylation, primarily resulting from phosphatases and kinases, leads to neurofibrillary tangles (NFTs), significantly impacting neuronal function. Asuni et al. found that immunization targeting the phosphorylated tau epitope can decrease tau aggregates and enhance motor performance in mice [10]. Dai et al. also treated AD mice with tau antibodies 43D and 77E9, resulting in a reduction of total tau levels and the alleviation of tau hyperphosphorylation at different phosphorylation sites, which led to memory and cognitive improvement in AD mice [11]. However, despite the numerous intervention methods targeting tau currently available, there has been a lack of significant breakthroughs in tau protein research, making the search for targets that affect tau protein an urgent need.

The mitochondria, essential organelles to all eukaryotic cells, participate in a multitude of biological processes [6]. Recent research has revealed a close relationship between mitochondrial dysfunction and

* Corresponding authors.
E-mail addresses: qc.zhuge@wmu.edu.cn (Q. Zhuge), haoqi.ni@wmu.edu.cn (H. Ni), lvxinhuang@wmu.edu.cn (X. Lv).
[1] These authors contributed equally to this work.

https://doi.org/10.1016/j.neurot.2024.e00353
Received 1 December 2023; Received in revised form 20 March 2024; Accepted 21 March 2024

abnormal phosphorylation of tau protein in AD patients. Post-mortem tissues from these patients have shown substantial impairments in mitochondrial function, along with significant alterations in mitochondrial morphology [5]. Furthermore, changes in mitochondrial function, encompassing disruptions in the electron transport chain and fusion-fission dynamics, lead to an increase in reactive oxygen species (ROS) and subsequent mitochondrial damage. ROS-mediated oxidative stress is known to promote Aβ deposition as well as abnormal phosphorylation of tau protein, thereby influencing AD progression [12–14]. Mitochondrial fusion and fission play a crucial role in abnormal tau phosphorylation. Drp1, a protein responsible for mitochondrial fission, is reduced in post-mortem hippocampal samples from AD patients and co-localizes with Aβ [15]. Proteins responsible for mitochondrial fusion, including MFN1, MFN2, and OPA1, are also diminished in these tissues [15,16]. Additionally, alterations in certain mitochondrial genes have been observed in the blood of early-stage AD patients [17]. Accumulating evidence also shows that changes in mitochondrial function can modulate the activity of serine/threonine protein kinase (AKT), ultimately leading to cellular autophagy and apoptosis [18]. Evandro et al. proposed that mitophagy, the removal of dysfunctional mitochondria, could reduce abnormal tau phosphorylation in AD patients, thereby delaying disease progression and improving cognition [19]. With many treatments focused on neuropathology proving unsuccessful, mitochondrial dysfunction has emerged as a promising novel target for AD treatment [20,21].

The enzyme encoded by Lars2 is a key factor in regulating mitochondrial protein synthesis and affecting the function of various proteins in the mitochondrial oxidative respiratory chain [22,23]. Lars2 is closely associated with diseases stemming from disruptions in the oxidative respiratory chain and the synthesis of mitochondrial proteins [24–26]. Recently, an increasing number of studies have shown its relevance to neurodegenerative diseases. Lars2 is reportedly downregulated in AD cases and induces leukodystrophy with a mitochondrial signature [27]. Additionally, changes in Lars2 function affect energy metabolism, epigenetic modifications, and cellular redox homeostasis, which in turn, can influence cell proliferation and apoptosis [24,28]. Lars2 has also been observed to modulate immune evasion in colorectal cancer and sideroblastic anemia [28,26]. Therefore, we hypothesize that Lars2 may influence tau protein phosphorylation in the neurodegenerative disease AD, subsequently impacting cognitive function in AD patients.

To further validate our hypothesis, we evaluated Lars2's role in neurodegenerative diseases, including Alzheimer's disease. We provided compelling evidence that Lars2 expression is elevated in AD and correlates with a poor prognosis. Furthermore, Lars2 could alter mitochondrial function. We demonstrated that Lars2 could influence glycogen synthase kinase 3 beta (GSK3β) expression via the PI3K-AKT pathway, ultimately affecting tau protein phosphorylation and exacerbating neurodegenerative changes in cellular and animal experiments. Overall, our findings suggest that Lars2 represents a potential target for AD metabolic therapy.

Materials and Measures

Animals and ethics consideration

Seven-month-old male APPswe/PSEN1De9 (APP/PS1) and C57BL/6J mice were obtained from GemPharmatech LLC. (Jiangsu, China). Adult B6/JGpt-Rosa25$^{emlCin\ (CAG\text{-}cas9\text{-}tdTomato)}$/Gpt mice (8–10 weeks old, 20–25 g) were also acquired from GemPharmatech LLC. (Jiangsu, China). Adult male and female C57BL/6 mice (8–10 weeks old, 20–25 g) were purchased from Shanghai Slaccas Experimental Animal Limited Liability Company (Shanghai, China). All animals were housed in a controlled environment with *ad libitum* access to food and water. Experimental procedures complied with the National Institutes of Health animal care and use guidelines and were approved by the Animal Ethics Committee at Wenzhou Medical University.

Cell culture and treatment

The Neuro-2a mouse neuroblastoma cell lines from ICell Bioscience Inc, Shanghai, and the HEK-293T engineered cells from the Cell Resources Center of the Shanghai Institute of Biosciences (Chinese Academy of Sciences, Shanghai, China) were cultured in Dulbecco's Modified Eagle Medium (DMEM, Gibco, 11995500, Waltham, MA, USA) supplemented with 10% fetal bovine serum (FBS, Gibco, 16000044, Waltham, MA, USA) and 1% penicillin-streptomycin (Gibco, 15070063, Waltham, MA, USA) within). Cells were maintained in a controlled incubator at 37 °C with 5% CO_2.

Primary cortical neurons acquired from pregnant C57BL/6 mice were cultured in Neurobasal™ Medium (Gibco, 21103049, Waltham, MA, USA). This medium was supplemented with 1% penicillin-streptomycin (Gibco, 15070063, Waltham, MA, USA), 1% B27™ Supplement (Gibco, 12587010, Waltham, MA, USA)), and 1% GlutaMAX™ (Gibco, 35050061, Waltham, MA, USA) within a controlled incubator environment set at 37 °C with 5% CO_2.

Okadaic acid (OA) was used in our *in vitro* cell model studies. For Neuro-2a and HEK293T cells, we used 20 nM OA for 12–24 h. For primary neuronal cells, we used 10 nM OA for 4 h.

Preparation of primary cortical neuron cultures

The preparation of cortical neuron cultures followed the methods described by Reddrop et al. and Samson et al. [29,30]. Briefly, C57BL/6 mice embryos were euthanized, and their brains were carefully removed and placed in a petri dish with cold Hanks' balanced salt solution (HBSS). Under a dissection microscope, the cortices were meticulously excised and transferred to another dish containing ice-cold HBSS. Blood vessels and meninges were thoroughly removed from the cortical tissue. The separated tissue was then trypsinized for 5 min at 37 °C, followed by trypsin inhibitor addition. The resulting cellular material was suspended in Dulbecco's Modified Eagle Medium (DMEM, Gibco, 11995500, Waltham, MA, USA), supplemented with 5% fetal bovine serum (FBS, Gibco, 16000044, Waltham, MA, USA) and 1% penicillin-streptomycin (all from Gibco, 15070063, Waltham, MA, USA). This cell suspension was then seeded into 12-well plates pre-coated with poly-D-lysine (0.05 mg/ml) at a density of 1.3 million cells per well. Four hours later, the serum-containing medium was removed and replaced with a serum-free neurobasal medium. Culture development was assessed daily by observing neurite outgrowth, and fresh medium (1:1) was added every two days.

Small interfering RNA and transfection

Small interfering RNA (siRNA) targeting mouse Lars2 and negative control (si-CON) were purchased from Sangon Biotech (Shanghai, China). siRNAs targeting human Lars2 and si-CON were obtained from Repobio (Hangzhou, China). Neuro-2a or HEK-293T cells were grown in 6-well plates to approximately 50% confluence at a density of 2×10^6 cells per well. Cells were then transfected with 20 μmol/ml of siLars2 or si-CON using 10 μl Lipofectamine RNAiMAX reagent (ThermoFisher) in DMEM at 37 °C for 24 h before okadaic acid (OA) treatment. Following the 24-h transfection period, cells were harvested for subsequent experiments. The siRNA sequences were displayed in Supplementary Table 2.

Plasmid construction and virus transfection

Lars2 knockdown (Lars2-KD1, Lars2-KD2) plasmids (pSLenti-U6-shRNA-CMV-EGFP-F2A-Puro-WPRE) and control vector were provided by Youze Biology (Changsha, China). P301L-tau441(MAPT P301L pcDNA3.1-His-C) was provided by RepoBio Biology (Hanzhou, China). Small guide RNA (sgRNA1, sgRNA2) plasmids (mLars2 sgRNA PX552)

and control vector were also provided by the same source. Lars2 overexpression (Lars2-OE) plasmids, both Lars2 PCDH-GFP-PURO-3 × Flag driven by CMV promoter and Lars2 pcDNA3.1-3 × Flag-C and their respective control vectors were obtained from Repobio (Hangzhou, China). Lentiviral vectors and packaging plasmids (pMDL, VSV-G, and pRSV) were transfected into HEK-293T cells, and the media were replaced after 16 h. At 24 and 48 h, viral media was collected, filtered, and supplemented with 10 ng/mL polybrene. Blinded investigators then used these prepared viruses to induce knockdown and overexpression of Lars2 in Neuro-2a cells and primary neuronal lines. Subsequent experiments were conducted after these manipulations.

Adeno-associated virus (AAV) production: HEK-293T cells were transfected with a combination of packaging plasmids (pAd-deltaF6 and pUCmini-iCAP-PHP.eB) and either a sgRNA plasmid or a control vector plasmid. On the third day, virus samples were obtained from both the cell lysates and the culture media. These samples underwent purification via iodixanol gradient ultracentrifugation, followed by washing with PBS and concentration using a 100K PES concentrator (Pierce™, Thermo Scientific). Virus titers were evaluated using quantitative PCR with ITR primers showed in Supplementary Table 2.

Protein extraction and western blot analysis

Total protein from glioma cells was extracted using RIPA lysis solution (Thermo Scientific, 89900, Waltham, MA, USA) supplemented with a protease phosphatase inhibitor cocktail (Beyotime, P1045, Shanghai, China) and phenylmethanesulfonyl fluoride (PMSF, Beyotime, ST506, Shanghai, China). Protein concentration was determined using a BCA protein assay kit (Thermo Scientific, 23227, Waltham, MA, USA). Subsequently, protein samples were separated via sodium dodecyl sulfate-polyacrylamide gel electrophoresis (SDS-PAGE) and transferred to polyvinylidene fluoride membranes (PVDF, Merck Millipore, IPFL85R, Darmstadt, Germany). Blocking was performed with a TBST (TBS, 0.1% Tween) solution containing 5% skimmed milk for 2 h at room temperature. This was followed by overnight incubation with primary antibodies at 4 °C. The details of the primary antibodies were displayed in Supplementary Table 1.

Sarkosyl insoluble tau purification and detection

Following the method of Longfei Li et al. [31], we conducted a Sarkosyl insoluble tau assay on HEK-293T-P301L cells. Briefly, the HEK-293T-P301L cells were subjected to either knockdown. The cells were then washed with PBS and lysed in RIPA buffer (Thermo Scientific, 89900, Waltham, MA, USA). Protein concentration was determined using the BCA method (Thermo Scientific, 23227, Waltham, MA, USA). The cell lysate was mixed with 1% sarkosyl (Glpbio, GC49092, Montclair, CA, USA) and incubated at room temperature for 1 h, followed by centrifugation at 100,000 g for 1 h at 4 °C. The precipitate (SI-tau) was washed once with the same buffer and resuspended in 1x loading buffer.

Animals

B6/JGpt-Rosa25$^{emlCin\ (CAG\text{-}cas9\text{-}tdTomato)}$/Gpt mice (n = 6) were anesthetized with isoflurane at 2% and placed in a stereotaxic apparatus (RWD Life Science, China). Following surgical standards for animal experiments, a 0.5-mm diameter bone window was drilled for injection (2 mm posterior to the bregma, 1.4 mm lateral to the midline, at a depth of 1.7 mm). The adeno-associated virus titer was diluted to 10^9 with PBS and injected using a Hamilton syringe, delivering 1 μL to one side (specify left or right) of the mouse hippocampus. After injection, the bone hole was closed with bone wax, and the scalp was operated on by the researchers. Subsequently, the mice were housed according to standard procedures. All measurements and observations were performed by a blinded researcher.

Behavior tests

Nest building was assessed in standard mouse cages with 1 cm thick padding and 30 evenly scattered 5 cm × 5 cm paper pieces. Each mouse was individually placed in a cage, and their nesting behavior was observed and documented through photographs after 12 h. The nesting score was assigned on a scale of 1–4, where: 1 = randomly scattered paper with no bite marks; 2 = an unformed nest with paper gathered on one side and no bite marks; 3 = a relatively flat nest with paper gathered on one side and several bite marks; 4 = a well-structured nest with extensive biting.

The novel object recognition test was conducted in a large, open cardboard box (40 cm × 40 cm × 40 cm), larger than a standard housing cage. Mice were first introduced to the box for 5 min of free exploration and acclimation. During training, they were placed in the box with two identical rectangular wooden blocks for 5 min. After a 24-h interval, one block was replaced by a cylindrical wooden block. Mouse exploration activities (sniffing, licking, and biting) toward the new and old objects were recorded via video analysis of the first 5 min of each session. To prevent odor cues, the box and blocks were cleaned with alcohol after each test. A consistent testing environment with subdued lighting was maintained throughout. The Recognition Index (RI = time spent exploring the new object/total exploration time) was calculated.

The Barnes maze was conducted on a 100 cm diameter circular workbench encircled by 20 evenly spaced escape holes, with a connected black escape box at one of the holes. The protocol spanned 6 consecutive days with three stages: adaptation (day 1), training (days 2–5), and testing (day 6). During adaptation, each mouse was physically led into the target hole and allowed to acclimate in the escape box for 4 min. In training, mice were placed in a 20 cm diameter, 27 cm high plastic cylinder at the maze's center and confined for 5 s. After cylinder removal, they searched for the escape box for 3 min, with the time taken for all four limbs to fully enter the target box recorded as latency. If a mouse could not find the target box within 3 min, the operator guided it in and allowed a 1-min stay. Mice received daily training on consecutive days. During testing, the workbench was divided into four quadrants, and the escape box was placed in the center of a designated quadrant. After removing the box, the time each mouse spent in the target quadrant was recorded and analyzed statistically. Before each test, the platform was randomly rotated to reposition the holes while the target box direction remained constant. All measurements and observations were performed by a blinded researcher.

Immunofluorescence staining and immunohistochemistry staining

Brain tissues were perfused through the left ventricle with 4% paraformaldehyde in PBS for immunohistochemistry. Post-perfusion, the tissue was processed for dehydration and fixation and then divided into frozen or paraffin sections. Initially, sections or cells were fixed in 4% paraformaldehyde for 20 min at room temperature. Blocking with PBST containing 5% BSA was performed for 30 min to minimize non-specific staining. Primary antibodies were then applied and incubated overnight at 4 °C. Subsequently, sections underwent secondary antibody treatment for 1 h at 37 °C. DAPI (Solarbio, S2110, Beijing, China) was used to stain the nuclei. Imaging was performed using a fluorescence microscope from Leica Microsystems, and analysis was conducted using ImageJ software. All assessments were carried out by a blinded investigator.

For immunohistochemical staining, brain tissues from APP/PS1 mice (AD models) underwent dewaxing and hydration. Subsequently, tissue sections were incubated in 3% H_2O_2 for 10 min to eliminate endogenous catalase. A citrate-EDTA antigen retrieval solution (Beyotime, P0086, Shanghai, China) was used to facilitate antigen restoration. Sections were then blocked with 5% BSA in PBST for 1 h at room temperature, followed by overnight incubation with primary antibodies at 4 °C. The next day, the sections were treated with HRP-labeled secondary antibodies for 1 h at 37 °C and then with DAB Color Development Kit (Beyotime, P0202,

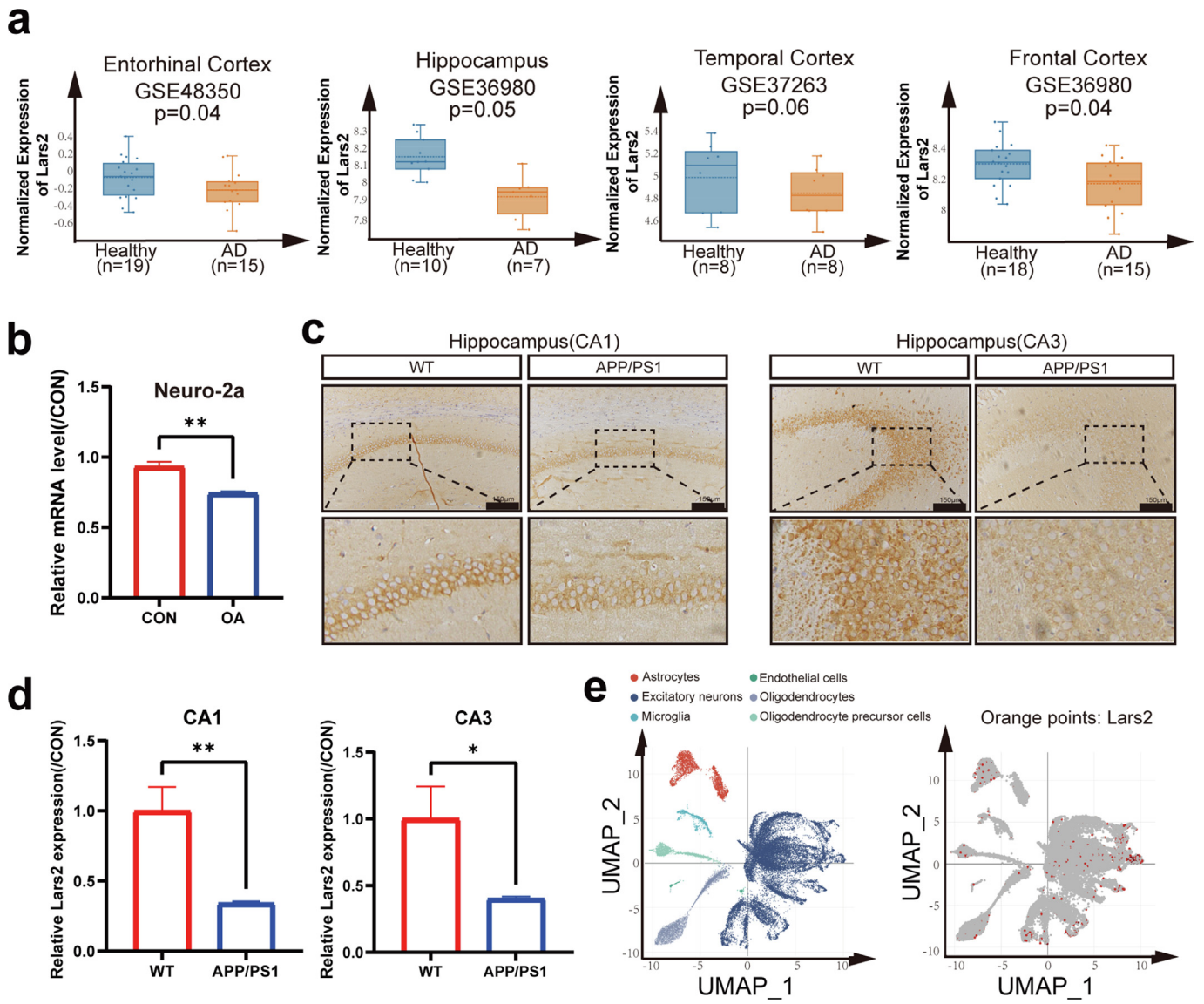

Fig. 1. Lars2 expression downregulated in AD. **(a)** The analysis of the Alzdata database revealed that Lars2 expression decreased in AD with multiple parts of the brain. **(b)** qRT-PCR analyzed the expression of Lars2 after Neuro-2a cells were treated by OA compared to the CON group (n = 3). **(c)** Immunohistochemistry was used to assess the expression of Lars2 in APP/PS1 compared to wild type (scale bar = 150 μm) (n = 4). **(d)** The quantification of Lars2 expression in the CA1 and CA3 (n = 4). **(e)** The Analysis of single-cell sequencing (scRNA-seq) of Human brain tissue was based on results of scREAD database (https://bmbls.bmi.osumc.edu/scread/). The differentiation of cell populations was based on the average expression of UMAP typical gene clusters (left) and Lars2 was expression across various brain cell types (right, Orange points). Data are presented as medians and interquartile ranges (a) or means ± SEM (b, d) and were analyzed by fisher's exact test (a) and student's *t*-test (b, d). (*$p < 0.05$; **$p < 0.01$).

Shanghai, China) for 5 min. Finally, the nuclei were counterstained with hematoxylin (Beyotime, C0107, Shanghai, China). All assessments and analyses were conducted by a blinded investigator. The primary antibodies used in this study were showed in Supplementary Table 1.

Real-time quantitative polymerase chain reaction (qRT-PCR)

Glioma cells underwent total RNA extraction using Trizol reagent (Thermo Scientific, 15596018, Waltham, MA, USA). Subsequently, cDNA libraries were constructed using the RevertAid RT reverse transcription kit (Thermo Scientific, k1691, Waltham, MA, USA). Quantitative real-time PCR (qRT-PCR) was performed using a 40-cycle program with the following steps: denaturation at 95 °C for 15 s, annealing at 60 °C for 15 s, and extension at 72 °C for 45 s. The cycle threshold (Ct) value of the target RNA was normalized to that of GAPDH. Finally, the relative expression was calculated using the $2^{-\Delta\Delta Ct}$ method. The qRT-PCR primer sequences were displayed in Supplementary Table 2.

Statistical analysis

All statistical analyses in this study were performed using GraphPad Prism 9. The student's *t*-test was applied to assess the normality of distribution between two data groups, while one-way ANOVA analysis was used to compare data among multiple groups. Homogeneity of variance was assessed using the Levene test. Data were presented as mean ± standard error of the mean (SEM). Statistical significance was defined as a two-tailed *p*-value <0.05.

Results

Lars2 expression downregulated in AD

The association between Lars2 expression and AD has been extensively documented. Leveraging data from the Alzdata database, we observed a downregulation of Lars2 expression across various brain

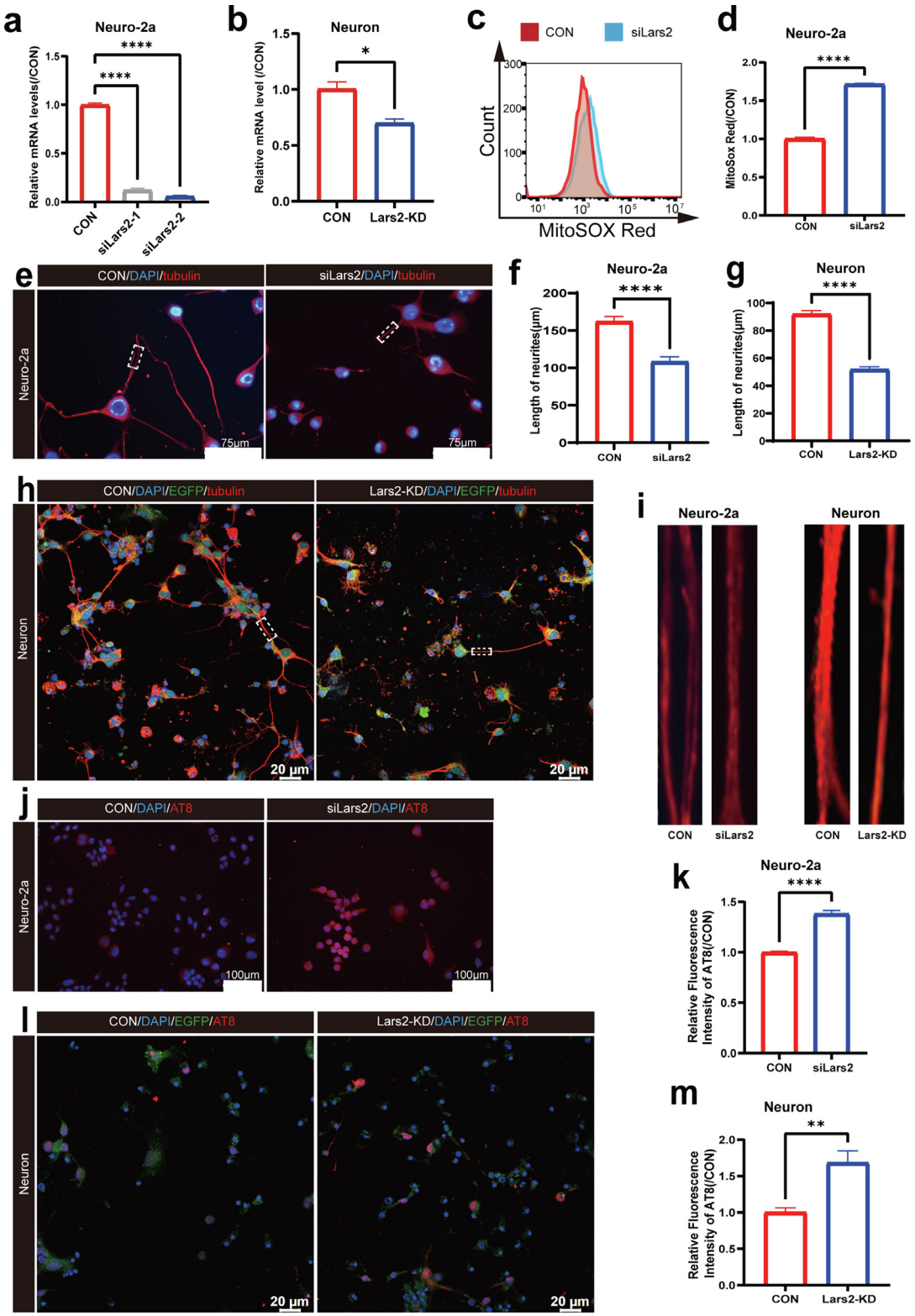

Fig. 2. Lars2 knockdown induced nerve injury and p-tau accumulation *in vitro* models. **(a)** qRT-PCR analyzed the knockdown efficiency of two different siRNA in Neuro-2a cell lines compared to the CON group (n = 3). **(b)** qRT-PCR analyzed the knockdown efficiency of LV-shLars2(Lars2-KD) in primary neurons compared to CON group (n = 3). **(c, d)** Flow cytometry detected the level of mitochondrial superoxide with siLars2 in Neuro-2a compared to the CON group. The mitochondrial superoxide levels were labeled by MitoSOX dye (n = 3). **(e, f)** Immunofluorescent detected the tubulin to analyze axon length in siLars2 Neuro-2a cells compared to the CON group (9 random fields from triplicate samples were captured for quantification) (scale bar = 75 μm). **(g, h)** Immunofluorescent detected the tubulin to analyze axon length in Lars2-KD primary neuron cells compared to the CON group (12 random fields from quadruplicate samples were captured for quantification) (scale bar = 20 μm). **(i)** Enlarged image of a specific region of axons. **(j, k)** Immunofluorescent detected AT8 (p-tau, S202/T205) expression in siLars2 Neuro-2a cells compared to the CON group (9 random fields from triplicate samples were captured for quantification) (scale bar = 100 μm). **(l, m)** Immunofluorescent detected AT8 (p-tau, S202/T205) expression in Lars2-KD primary neuron cells compared to the CON group. (12 random fields from quadruplicate samples were captured for quantification) (scale bar = 20 μm). All data are presented as means ± SEM and were analyzed by student's *t*-test or One-way ANOVA. (*$p < 0.05$; **$p < 0.01$; ****$p < 0.0001$).

regions in AD patients in some individual studies, including the entorhinal cortex (GSE48350), hippocampus (GSE36980), temporal cortex (GSE37263) and frontal cortex (GSE36980) (Fig. 1a). (Link to Alzdata: https://www.alzdata.org/). Further investigation at the cellular level revealed a marked reduction in Lars2 mRNA levels upon treatment of Neuro-2a cells with okadaic acid for 24 h, as quantified by qPCR analysis. It is well-established that OA treatment can be used to establish an *in vitro* model of AD (Fig. 1b). Transgenic APP/PS1 mice subjected to immunohistochemical analysis demonstrated diminished Lars2 expression in both the CA1 and CA3 regions of the hippocampus compared to wild-type mice (Fig. 1c and d). To further understand the cellular distribution of Lars2 expression within the brain, we analyzed data from the scREAD database (AD00201) (Link to scREAD: https://bmbls.bmi.osumc.edu/scread/). After optimizing SNN(Shared Nearest Neighbour) resolution parameters through contour analysis, the clusters were interpreted as broadly defining 6 distinct cell populations based on the cluster average expression of typical genes by UMAP(Uniform Manifold Approximation and Projection) (Fig. 1e, left). Further analysis showed that Lars2 was expression across various brain cell types, including excitatory neurons. (Fig. 1e, right, orange points).

Lars2 knockdown increases nerve damage and p-tau accumulation in vitro models of cells

To investigate this further, we generated Lars2 knockdown models in Neuro-2a cells using siLars2-1, siLars2-2, and siLars2-CON small interfering RNAs (siRNAs) or short hairpin RNAs (shRNAs). Knockdown efficiency was validated by qPCR (Fig. 2a, Sup. 2a). Cell viability assays using a Cell Counting Kit-8 (CCK8) revealed a significant decrease in Neuro-2a cells with Lars2-KD1 and Lars2-KD2 compared to controls (Sup. 2b). Due to similar knockdown efficiency, Lars2-KD1 and siLars2-1 were chosen for subsequent experiments. Knockdown of Lars2 was also established in primary neurons with validation by qPCR (Fig. 2b). Mitochondrial superoxide levels, indicated by the MitoSOX fluorescence probe, were significantly increased in OA-treated cells and further exacerbated by Lars2 knockdown (Fig. 2c and d, Sup. 1c, d), suggesting a substantial impact on cellular mitochondrial function. To assess the effects of Lars2 knockdown on neuronal morphology, Neuro-2a cells were cultured with 20 μM retinoic acid (RA) and 1% serum for 48 h. Immunofluorescence staining with tubulin antibodies revealed significantly shorter axon lengths and fewer dendritic branches in siLars2-treated Neuro-2a cells compared to controls (Fig. 2e, f, i). Similar results were observed in primary neurons with Lars2-KD, highlighting the significant impact of Lars2 on neuronal function (Fig. 2g, h, i). Additionally, staining with Hoechst and PI dyes revealed varying degrees of increased cell death in both Neuro-2a cells and primary neurons following Lars2-KD (Sup. 2d, e, f, g), indicating a significant contribution of Lars2 knockdown to neuronal and neuron-like cell damage.

It is now understood that in neurodegenerative diseases, elevated levels of phosphorylated tau protein (p-tau) lead to the entanglement of nerve fibers and disruption of neuronal function, making it a crucial marker of these pathologies. Therefore, we employed immunofluorescence staining to quantify the expression of p-tau phosphorylated at S202/T205 in both Neuro-2a cells and primary neurons. Our results consistently demonstrated that OA treatment increased the phosphorylation level of tau S202/T205 in Neuro-2a cells (Sup. 1a, b). Furthermore, Lars2 knockdown significantly exacerbated this effect, leading to a marked elevation in p-tau expression in both Neuro-2a cells and primary neurons (Fig. 2j, k, l, m).

Lars2 knockdown alters the morphology and function of mitochondria in neuron-like cells

Current evidence suggests that Lars2, encoding a synthetase for mitochondrial leucine tRNA, regulates mitochondrial protein synthesis and ultimately affects the function of various proteins in the mitochondrial oxidative respiratory chain. Using the MitoTracker fluorescent probe and laser confocal microscopy, we observed significant changes in mitochondrial shape and overall cell morphology in Neuro-2a cells after Lars2 knockdown with siLars2. Compared to the negative control, mitochondria appeared sparser, shorter, and less branched (Fig. 3a). Furthermore, we established that Lars2 knockdown could significantly influence mitochondrial superoxide production (Fig. 2c and d). Based on these findings, it is highly conceivable that Lars2 knockdown significantly impacts mitochondrial function. To investigate this hypothesis further, we employed the JC-1 fluorescent probe to assess changes in mitochondrial membrane potential (MMP). Both microscopic observation and flow cytometry analysis revealed a notable decrease in MMP in Neuro-2a cells following siLars2 (Fig. 3b, c, d). Given the high energy and oxygen demands of neurons, along with mitochondria being the primary site of ATP generation, we hypothesized that Lars2 knockdown could impact ATP production. Consistent with this hypothesis, an ATP Assay Kit detected a significant decrease in ATP levels with siLars2 (Fig. 3e). Finally, we examined changes in mitochondrial complexes and associated structural proteins using Western blot analysis. Notably, we observed minimal changes in both mitochondrial complexes (Fig. 3f and h) and related mitochondrial structural proteins (Fig. 3g and i) following Lars2 knockdown. These experiments collectively demonstrate the significant influence of Lars2 on mitochondrial function in neurons, which ultimately impacts neuronal cell functionality.

Lars2 regulates p-tau accumulation by targeting the PI3K-AKT-GSK3β pathway

To elucidate the mechanisms underlying neurodegenerative changes after Lars2 knockdown, we performed transcriptome sequencing on total RNA isolated from control and siLars2 Neuro-2a cells. The top 25 up- and down-regulated genes demonstrated significant alterations in the cellular transcriptome (Fig. 4a). Additionally, a volcano plot (fold change $\geq$1.1 and *p*-adjusted value < 0.05) visualized the differential gene expression changes (Fig. 4b). KEGG(Kyoto Encyclopedia of Genes and Genomes, http://www.genome.jp/kegg/) enrichment analysis revealed a significant enrichment of the phosphatidylinositol 3-kinase/protein kinase B (PI3K-AKT) pathway upon Lars2 knockdown (*p*-adjusted value < 0.05 for FDR, Fig. 4c). Knockdown efficiency of siLars2-1 and siLars2-2 in HEK-293T cells treated with OA was confirmed by qPCR (Sup. 2c), and siLars2-1 was chosen for subsequent experiments due to similar knockdown efficiency. qPCR analyses of serine/threonine protein kinase 1 (AKT1), 2 (AKT2), 3 (AKT3), and downstream glycogen synthase kinase 3 beta (GSK3β) revealed decreased mRNA expression in the Lars2 knockdown group compared to the control (Fig. 4d). Western blot confirmed relevant protein changes in Lars2 knockdown cells treated with OA: decreased total AKT and phosphorylated AKT (p-AKT), increased GSK3β, and significantly decreased phosphorylated GSK3β (S9) (Fig. 4e and f). To further clarify the effect of down-regulating Lars2 on tau, we used HEK-293T cells transfected with P301L-Tau441 plasmid (P301L cells) as an *in vitro* model to study AD tau phosphorylation. Additionally, p-tau (T181/S202/T205/S396) was significantly increased in P301L cells with Lars2 knokdown by siRNA (Fig. 4g and h). However, it is observed that there is no significant change in the proportion of sarkosyl-insoluble tau in total tau after Lars2 knockdown (Sup 3a, b). Collectively, these findings provide compelling evidence that Lars2 influences neuronal function through the PI3K-AKT axis.

Lars2 overexpression reversed neuronal injury and tau phosphorylation in the vitro model of AD

To verify the mechanism by which Lars2 influences AD pathology, Lars2 was overexpressed in HEK-293T cells. Western blot analysis confirmed the expression of the overexpressed Lars2 (Sup. 3c, d). Following treatment with OE-Lars2 or OE-FLAG, HEK-293T cells were incubated with 20 nM OA for 12 h. JC-1 fluorescent probes were used to

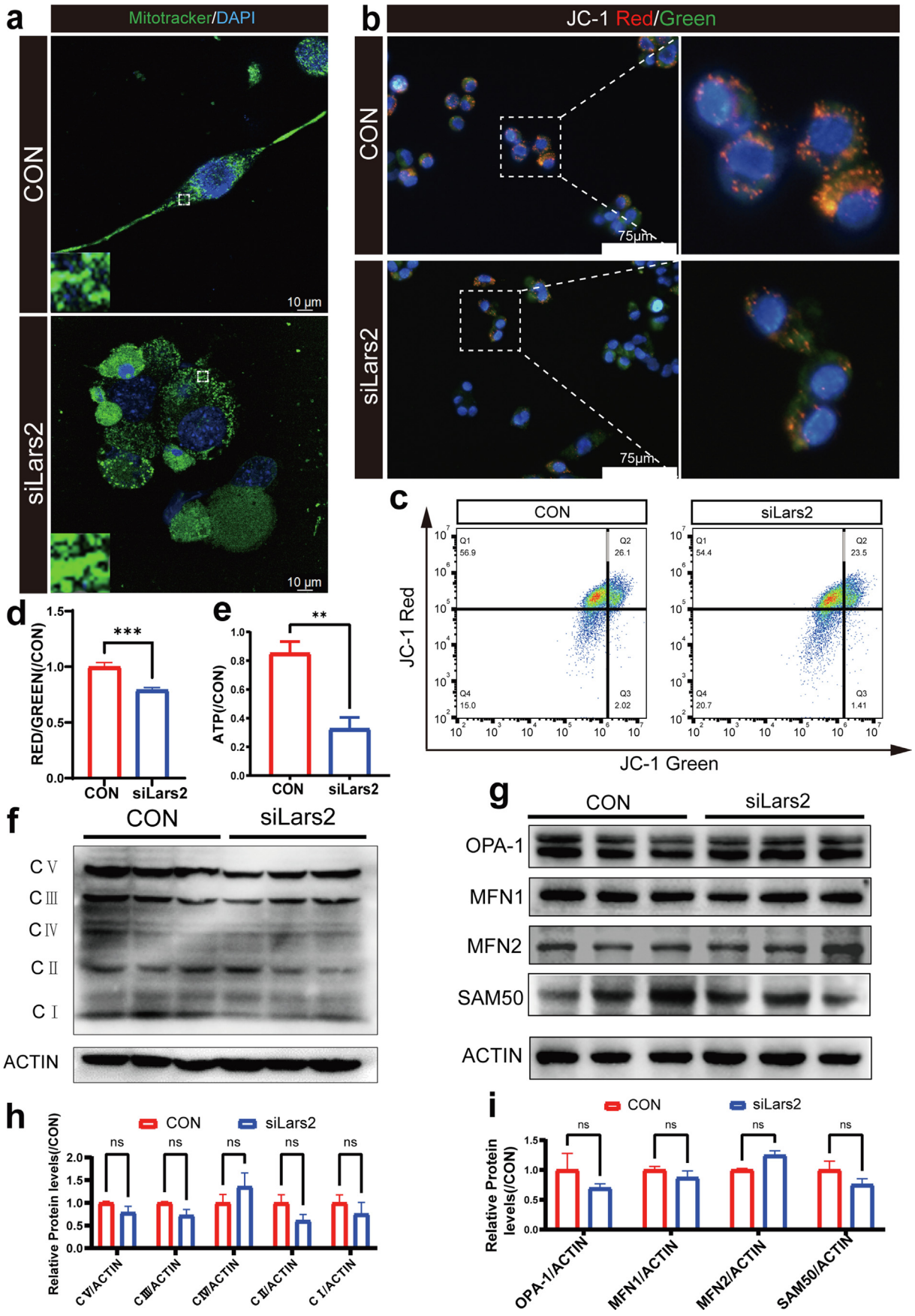

(caption on next page)

measure MMP in HEK-293T cells. Notably, Lars2 overexpression mitigated the changes in MMP induced by OA (Fig. 5a and b). Similarly, using MitoSOX fluorescent probes to assess mitochondrial superoxide changes, we found that Lars2 overexpression reversed the OA-induced alterations in mitochondrial superoxide levels (Fig. 5c and d). Western blot experiments further revealed that Lars2 overexpression reversed the changes induced by OA in relevant proteins, including p-AKT/AKT, p-GSK3β/GSK3β in HEK-293T cells (Fig. 5e and f). In addition, Lars2 overexpression also reversed the changes of p-tau(S202/T205)/tau, p-tau(T181)/tau, p-tau(S396)/tau in P301L cells (Fig. 5g and h).

To investigate the impact of Lars2 overexpression on AD pathology, we used an *in vitro* model of tauopathy induced by OA in primary neurons and Neuro-2a cells. Cells were incubated with OA at appropriate concentrations (10 nM for primary neurons for 4 h, and 20 nM for Neuro-2a cells for 12 h) based on their different sensitivities (experimental diagram in Fig. 6a). We then assessed the effects of Lars2 overexpression on neuronal morphology and tau phosphorylation. Tubulin immunostaining revealed that Lars2 overexpression reversed the OA-induced alterations in axon length and dendritic branching in both Neuro-2a cells and primary neurons (Fig. 6b, c, d, e). Additionally, immunofluorescence staining of both cell types demonstrated that Lars2 overexpression counteracted the increase in phosphorylated tau at Ser202/Thr205 expression caused by OA (Fig. 6f, g, h, i). These findings suggest that Lars2 overexpression can reverse neurodegenerative changes in neurons, supporting its potential as a therapeutic target for AD.

The Lars2 targeted knockout in hippocampal neurons by CRISPER-Cas9 induced cognitive decline in mice and p-tau accumulation

To further investigate the impact of Lars2 knockout on neurons, we used B6/JGpt-Rosa25$^{emlCin\ (CAG\text{-}cas9\text{-}tdTomato)}$/Gpt mice. Purified and concentrated adenoviruses were bilaterally injected into the hippocampus, followed by behavioral testing four weeks post-injection. Brain slices were obtained eight weeks post-injection for relevant immunofluorescence staining (Fig. 7a). The Barnes maze test revealed significant cognitive impairment in mice after Lars2 knockout, as evidenced by increased latency time and target quadrant time (Fig. 7b and c). Similarly, the novel object recognition experiment demonstrated a cognitive decline in Lars2 knockout mice using the recognition index (Fig. 7d). Nest building tests showed a marked reduction in nest scores after Lars2 knockout (Sup. 4a, b). To verify the efficiency of adenovirus-mediated Lars2 knockout in hippocampal neurons, we used immunofluorescence staining. Reduced Lars2 expression was observed at sites of adenoviral infection (EGFP), while uninfected regions showed no significant change (Fig. 7e). Immunofluorescence staining was also used to assess phosphorylated tau at Ser202/Thr205 expression levels and investigate the impact of Lars2 knockout *in vivo*. We observed a notable increase in phosphorylated tau at Ser202/Thr205 expression in the hippocampus of Lars2 knockout mice compared to the control group (Fig. 7f and h). Finally, immunofluorescence revealed a significant reduction in hippocampal area in the same coronal plane of Lars2 knockout mice compared to controls (Fig. 7g and i). These findings collectively suggest that Lars2 knockout leads to elevated p-tau expression in neurons, ultimately resulting in neurodegenerative changes.

Discussion

Our study focused on investigating the impact of Lars2 manipulation on neurodegenerative changes, suggesting a promising avenue for clinical AD treatment. *In vitro* experiments revealed that Lars2 knockdown increased neuronal cell death, disrupted mitochondrial function, and negatively affected neuronal axonal length and cellular p-tau expression. Consistent *in vivo* findings were observed, where Lars2 knockdown in mice led to substantial behavioral changes and cognitive decline. Furthermore, hippocampal neurons in these mice exhibited trends similar to those observed *in vitro*. Mechanistically, we identified that Lars2 knockdown inhibited the activation of the PI3K-AKT pathway, leading to GSK3β dephosphorylation and ultimately contributing to increased p-tau expression.

Lars2, an enzyme responsible for attaching leucine to its corresponding tRNA, is crucial for mitochondrial protein synthesis [32]. This process, known as charging tRNALeu(UUR) with leucine, is essential for mitochondrial function [23,33]. While most mitochondrial aminoacyl-tRNA synthetase-related diseases indirectly impact the central nervous system (CNS) through their role in maintaining the mitochondrial genome [34–36], Lars2, as a synthase specific to mitochondrial leucine-tRNA, directly affects mitochondrial function [37]. Our study validated that Lars2 knockdown could significantly alter mitochondrial morphology in Neuro-2a cells, impacting both membrane potential and the expression of mitochondrial complexes and associated proteins. Mitochondria, vital for energy production, are also known sources of ROS. Elevated ROS levels are implicated in the pathogenesis of various neurodegenerative disorders, including AD. Reduced Lars2 expression compromises the mitochondrial stress response, leading to increased ROS levels [22]. Our findings suggest a distinct role for Lars2 in influencing mitochondrial function, primarily impacting complex protein expression rather than structural protein composition. While previous studies suggest that functional abnormalities in mitochondrial complexes can lead to structural alterations, further investigation is warranted to confirm this link in the context of Lars2. Intriguingly, studies have shown that changes in mitochondrial function can intensify tau protein phosphorylation, a key target in AD treatment, although the specific *mechanisms remain unclear* [38–41]. Our experiments demonstrate that Lars2 knockdown not only affects Neuro-2a cell axon length but also leads to increased p-tau expression. Additionally, research suggests that Lars2 modulates apoptosis in ovarian granulosa cells through mitochondrial regulation [22,32]. Taken together, this evidence highlights the significant influence of Lars2 on mitochondrial function. By influencing ROS production and potentially impacting complex protein function, Lars2 may contribute to elevated p-tau expression and, ultimately, AD progression.

GSK3β, a serine-threonine kinase, is implicated in AD progression. Its activation stimulates tau hyperphosphorylation, leading to neurofibrillary tangles and amyloid plaques [42–44]. In recent years, GSK3β inhibitors have been explored as potential AD treatments [45]. Notably, GSK3β, a direct downstream target of AKT, is inhibited by phosphorylation at Ser9 by AKT [46,47]. Our RNA sequencing results identified significant enrichment of the AKT pathway in differentially expressed genes (DEGs) between Lars2 knockdown and control groups based on KEGG analysis. This finding prompted us to further investigate the

Fig. 3. Lars2 knockdown altered the morphology and function of mitochondria in neuron-like cells. **(a)** Confocal laser microscopy detected the mitochondrial morphology in siLars2 neuro-2a cells compared to the CON group. MitoTracker dye-labeled the mitochondrial morphology (scale bar = 10 μm). **(b)** Fluorescence microscopy detected the mitochondrial membrane potential levels in siLars2 Neuro-2a cells compared to the CON group (scale bar = 75 μm). JC-1 dye-labeled the mitochondrial membrane potential. **(c, d)** Flow cytometry detected the mitochondrial membrane potential levels compared to the CON group (n = 3). JC-1 dye-labeled the mitochondrial membrane potential. **(e)** ATP detection assay kit detected the ATP levels in siLars2 Neuro-2a cells compared to the CON group (n = 3). **(f, h)** Western blot analyzed the mitochondrial complex protein in siLars2 Neuro-2a cells compared to the CON group (n = 3). **(g, i)** Western blot analyzed of OPA-1, MFN1, MFN2 and SAM50 protein in siLars2 Neuro-2a cells compared to the CON group (n = 3). All data are presented as means ± SEM and were analyzed by student's *t*-test. (**$p < 0.01$; ***$p < 0.001$).

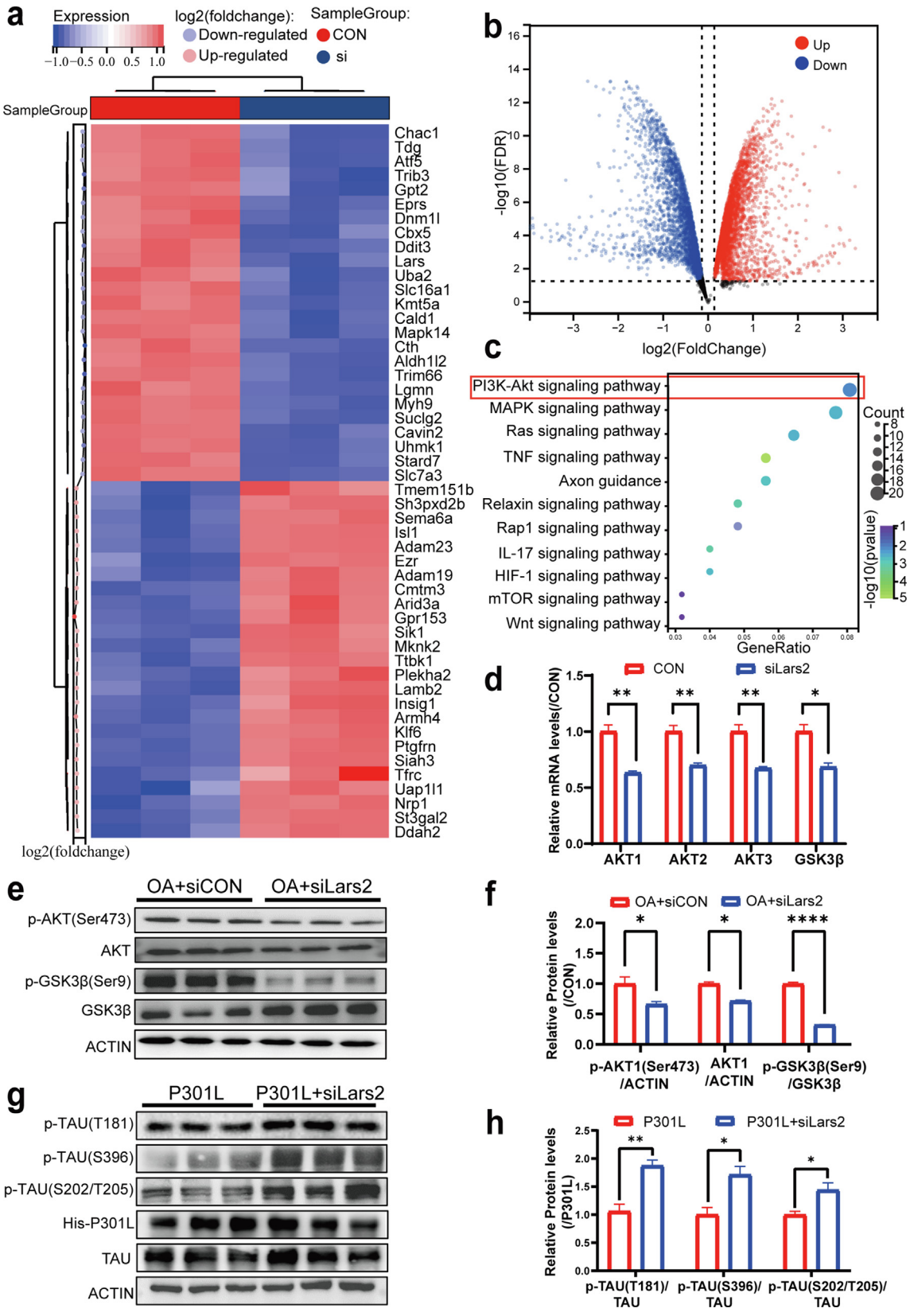

Fig. 4. Lars2 induced p-tau accumulation by targeting the PI3K-AKT-GSK3β pathway. **(a)** Heatmap of the expression of 50 distinct genes in siLars2 Neuro-2a cells compared to the CON group (n = 3). **(b)** Volcano plot depicting the changes in gene expression between the CON group and siLars2 Neuro-2a cells (fold change = 1.1, *p*-adjusted value < 0.05). **(c)** KEGG pathway enrichment verified the expression of pathways. The pathways were ranked by *p*-adjusted value < 0.05 for FDR. **(d)** qRT-PCR detected the pathway related mRNA levels in siLars2 HEK-293T cells compared to CON group (n = 3). **(e, f)** Western blot analysis of p-AKT(ser473), AKT, p-GSK3β(ser9), GSK3β in siLars2 HEK-293T cells (n = 3). **(g, h)** Western blot analysis of p-tau(S202/T205), p-tau(T181), p-tau(S396) and tau protein in siLars2 P301L cells (n = 3). All data are presented as means ± SEM and were analyzed by student's *t*-test. (*$p < 0.05$; **$p < 0.01$; ****$p < 0.0001$).

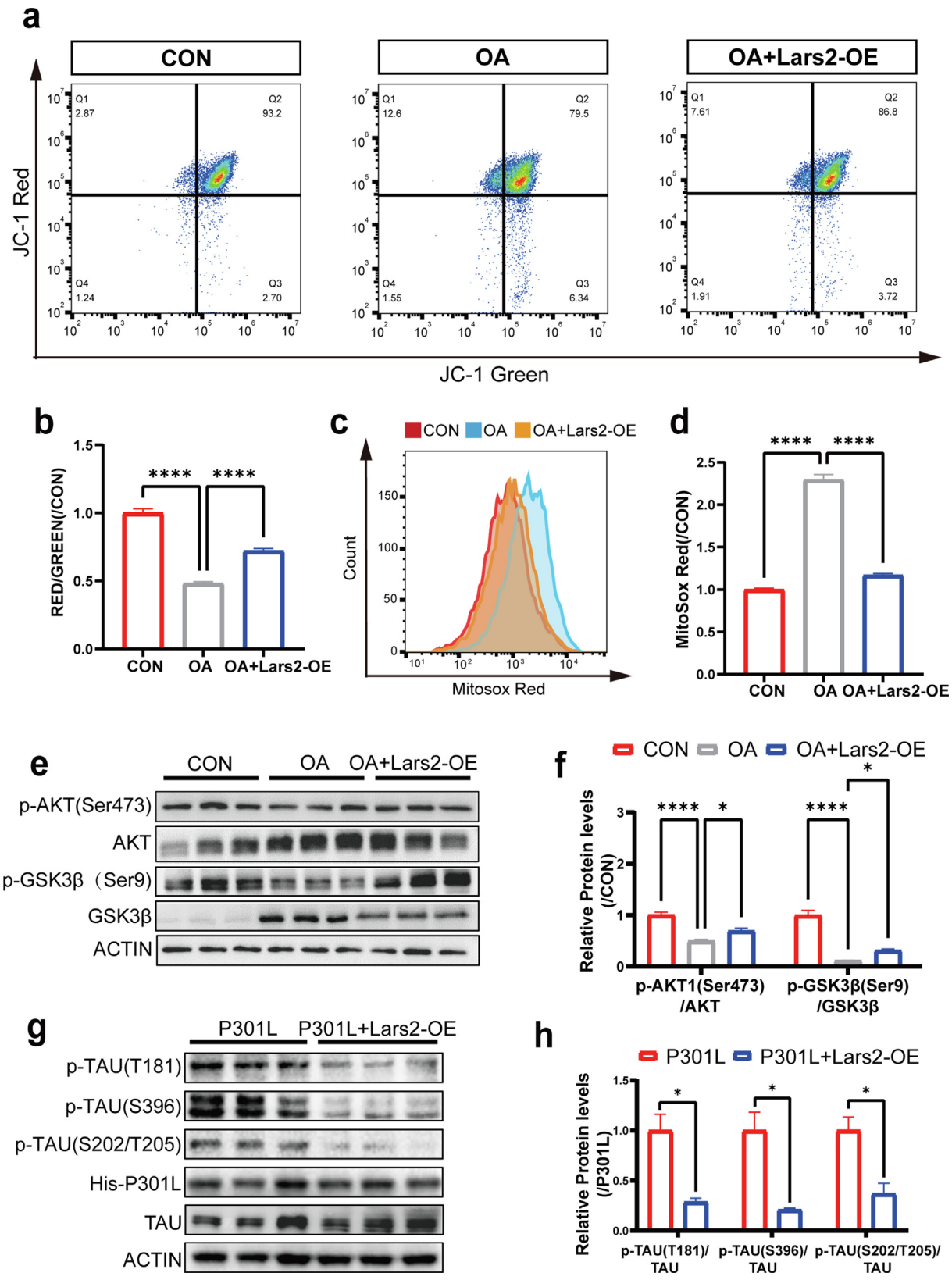

Fig. 5. Lars2 overexpression reversed mitochondrial injury and tau phosphorylation *in vitro* model of AD. **(a, b)** Mitochondrial membrane potential was assessed in HEK-293T cells treated with OA alone or co-treated with OA and Lars2 overexpression (OA + Lars2-OE) using JC-1 dye. Flow cytometry analysis quantified mitochondrial membrane potential levels (n = 3). **(c, d)** Mitochondrial superoxide levels were measured in HEK-293T cells treated with OA alone or OA + Lars2-OE using MitoSOX dye. Flow cytometry analysis quantified mitochondrial superoxide levels (n = 3). **(e, f)** Western blot analysis of key proteins involved in the PI3K-AKT-GSK3β-tau pathway was performed in HEK-293T cells treated with OA alone or OA + Lars2-OE. Proteins analyzed include phosphorylated AKT (p-AKT, Ser473), total AKT, phosphorylated GSK3β (p-GSK3β, Ser9), total GSK3β (n = 3). **(g, h)** Western blot analysis of p-tau(S202/T205), p-tau(T181), p-tau(S396) and tau protein in Lars2-OE P301L cells (n = 3). All data are presented as means ± SEM and were analyzed by student's *t*-test or One-way ANOVA. (*$p < 0.05$; ****$p < 0.0001$).

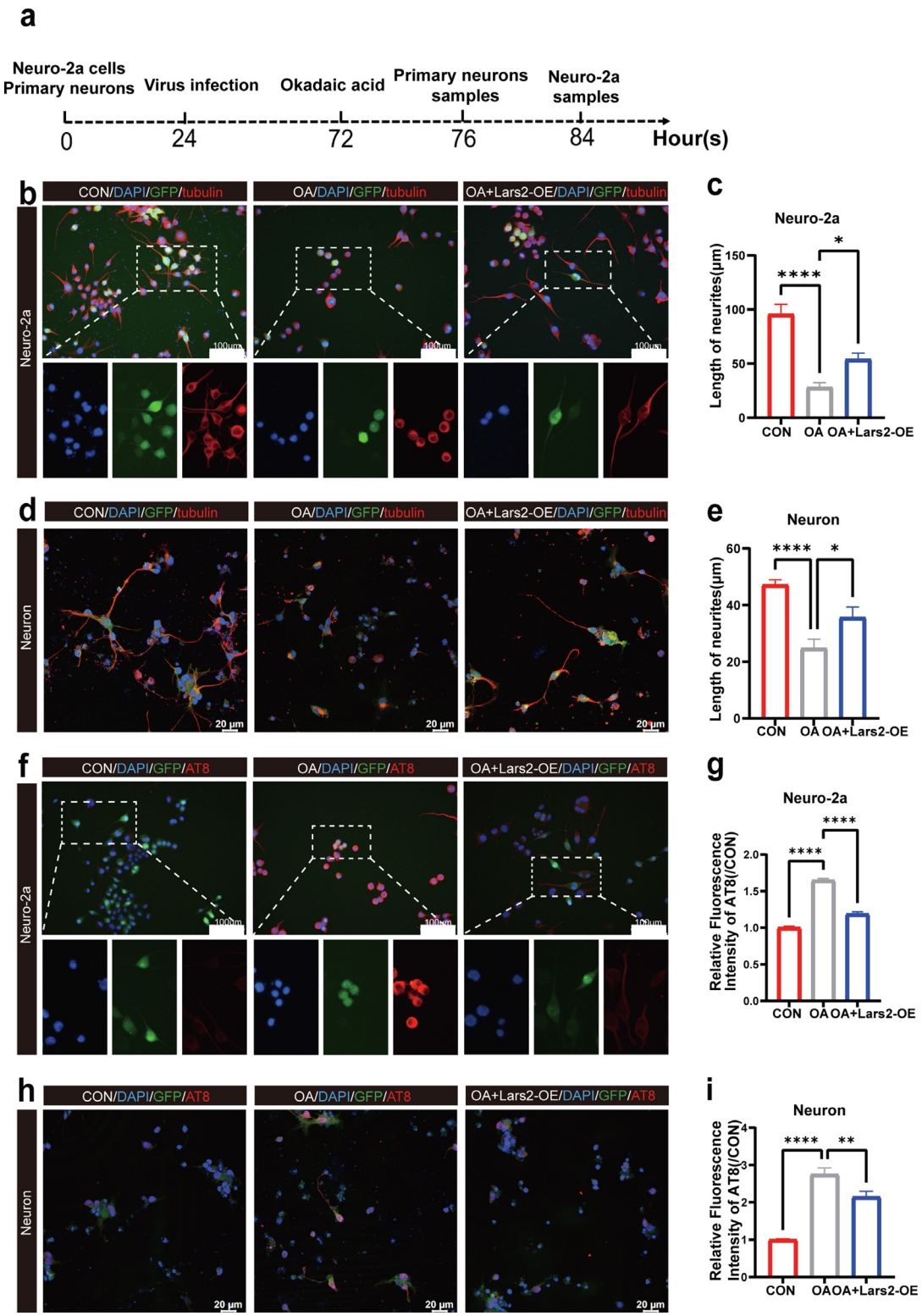

Fig. 6. Lars2 overexpression mitigated neuronal injury and p-tau accumulation in an *in vitro* model of AD. **(a)** Timeline of the experiment, including Neuro-2a cells and primary neurons. **(b, c)** Immunofluorescence staining for tubulin was performed to analyze axon length in Neuro-2a cells treated with Okadaic Acid (OA) alone or co-treated with OA and Lars2 overexpression (OA + Lars2-OE). (9 random fields from triplicate samples were captured for quantification) (scale bar = 100 μm). **(d, e)** Immunofluorescence staining for tubulin was performed to analyze axon length in primary neurons treated with OA or OA + Lars2-OE (9 random fields from triplicate samples were captured for quantification) (scale bar = 20 μm). **(f, g)** Immunofluorescence staining for AT8 (p-tau, S202/T205) was used to assess its expression in OA-treated Neuro-2a cells compared to OA + Lars2-OE (12 random fields from quadruplicate samples were captured for quantification) (scale bar = 100 μm). **(h, i)** Immunofluorescence staining for AT8 (p-tau, S202/T205) expression in OA + Lars2-OE primary neurons compared to OA group (9 random fields from triplicate samples were captured for quantification) (scale bar = 20 μm). All data are presented as means ± SEM and were analyzed by One-way ANOVA. (*$p < 0.05$; **$p < 0.01$; ****$p < 0.0001$).

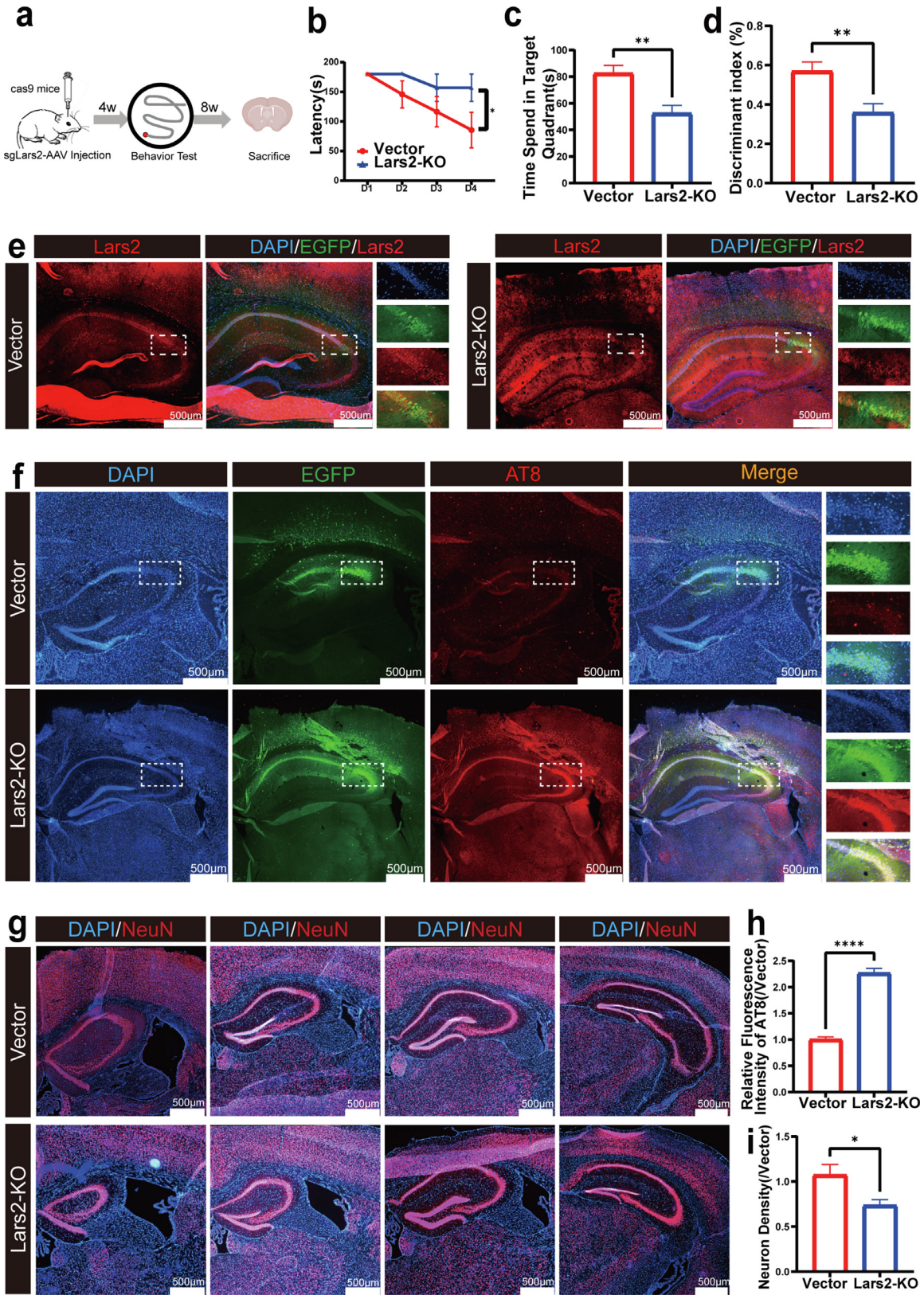

Fig. 7. Lars2 Knockout in Hippocampal Neurons induced cognitive decline and p-tau accumulation in mice. **(a)** Timeline of the experiment, including viral injections and behavioral testing. **(b, c)** Assessment of cognitive function in Lars2 knockout mice compared to controls using the Barnes maze test (n = 6 mice). **(d)** Novel object recognition test to evaluate cognitive performance in Lars2 knockout mice compared to controls (n = 6 mice). **(e)** Dual immunofluorescence staining showing viral infection (green) and Lars2 expression (red) in the hippocampus (scale bar = 500 μm). **(f, h)** Immunofluorescence staining for AT8 (p-tau, S202/T205) in the hippocampus of Lars2 knockout mice compared to controls (n = 6 mice) (scale bar = 500 μm). **(g, i)** Quantitative analysis of hippocampal size of Lars2 knockout mice compared to controls. Immunofluorescence staining for NeuN (neuronal marker) shows neuronal distribution. Hippocampal area was measured in the same coronal plane (n = 6 mice) (scale bar = 500 μm). All data are presented as means ± SEM and were analyzed by student's *t*-test. (*$p < 0.05$; **$p < 0.01$; ****$p < 0.0001$).

potential of Lars2 to modulate GSK3β inhibition by influencing the PI3K-AKT pathway. Our experiments confirmed that decreased Lars2 expression leads to inhibited AKT activity, resulting in increased GSK3β activity and, ultimately, elevated p-tau levels.

The PI3K-AKT pathway plays a crucial role in various cellular signaling processes [48]. Activation of this pathway leads to AKT-mediated phosphorylation and subsequent deactivation of GSK3β [49]. Studies suggest that optimal levels of ROS are necessary for PI3K-AKT activation, while excessive ROS accumulation can inhibit AKT activity [50,51]. Notably, ROS can directly activate phosphatase and tensin homolog (PTEN), a negative regulator of PI3K-AKT signaling, by oxidizing cysteine residues within its active center, ultimately suppressing AKT activation [51,52]. These findings align with our observations. While our study demonstrates significant alterations in mitochondrial function following Lars2 knockdown, further evidence is needed to establish a direct link between Lars2 and ROS levels. However, we have confirmed that Lars2 can reduce p-tau levels through its potential modulation of the PI3K-AKT-GSK3β axis.

Our investigation demonstrated that Lars2 influences alterations in neuronal mitochondria, leading to a significant increase in ROS. This elevated ROS level suppresses AKT activity, diminishing its inhibitory effect on the downstream target GSK3β. Consequently, GSK3β activity increases, resulting in elevated p-tau levels and ultimately contributing to damage in neuronal morphology and function. While research on regulatory genes of mitochondria in AD remains limited, our findings demonstrate that changes in Lars2 expression can impact AD progression. This suggests Lars2 as a potential novel target for clinical intervention in AD therapy.

Data Availability

The datasets used during the study are available from the corresponding author on request.

Funding

The work was supported by National Naturel Science Foundation of China (82271345 to QZ).

Author Contributions

XL, HN, and QZ designed the experiments and edited the manuscript. WQ, WZ, and LG conducted the *in vivo* experiments and performed the statistical analyses. WQ, WZ, LY, and YC carried out the *in vitro* experiments and the associated statistical analyses. XL and LY analyzed the Alzdata database and RNA-seq results. The first draft of the manuscript was written by WQ. All authors have read and agreed to the published version of the manuscript.

Declaration of competing interest

The authors declare that they have no known competing financial interests or personal relationships that could have appeared to influence the work reported in this paper.

Acknowledgments

We thank the Scientific Research Center of Wenzhou Medical University for providing the confocal microscopy. The authors express gratitude to Dr. Peng Zhang from Wenzhou Medical University and Dr. Cifeng Cai from Hangzhou Cosmos Wisdom for their technical support in data analysis and review.

Appendix A. Supplementary data

Supplementary data to this article can be found online at https://doi.org/10.1016/j.neurot.2024.e00353.

References

[1] Lane CA, Hardy J, Schott JM. Alzheimer's disease. Eur J Neurol 2018;25(1):59–70.
[2] Zhao LG, Tang Y, Tan JZ, Wang JW, Chen GJ, Zhu BL. The effect of NR4A1 on APP metabolism and tau phosphorylation. Genes Dis 2018;5(4):342–8.
[3] Crews L, Masliah E. Molecular mechanisms of neurodegeneration in Alzheimer's disease. Hum Mol Genet 2010;19(R1):R12–20.
[4] Sanabria-Castro A, Alvarado-Echeverría I, Monge-Bonilla C. Molecular pathogenesis of Alzheimer's disease: an update. Ann Neurosci 2017;24(1):46–54.
[5] Hoyer S. Oxidative energy metabolism in Alzheimer brain. Studies in early-onset and late-onset cases. Mol Chem Neuropathol 1992;16(3):207–24.
[6] Nunnari J, Suomalainen A. Mitochondria: in sickness and in health. Cell 2012;148(6):1145–59.
[7] Pérez MJ, Jara C, Quintanilla RA. Contribution of tau pathology to mitochondrial impairment in neurodegeneration. Front Neurosci 2018;12:441.
[8] Chong FP, Ng KY, Koh RY, Chye SM. Tau proteins and tauopathies in Alzheimer's disease. Cell Mol Neurobiol 2018;38(5):965–80.
[9] Amadoro G, Ciotti MT, Costanzi M, Cestari V, Calissano P, Canu N. NMDA receptor mediates tau-induced neurotoxicity by calpain and ERK/MAPK activation. Proc Natl Acad Sci USA 2006;103(8):2892–7.
[10] Asuni AA, Boutajangout A, Quartermain D, Sigurdsson EM. Immunotherapy targeting pathological tau conformers in a tangle mouse model reduces brain pathology with associated functional improvements. J Neurosci 2007;27(34):9115–29.
[11] Dai CL, Chen X, Kazim SF, Liu F, Gong CX, Grundke-Iqbal I, et al. Passive immunization targeting the N-terminal projection domain of tau decreases tau pathology and improves cognition in a transgenic mouse model of Alzheimer disease and tauopathies. J Neural Transm 2015;122(4):607–17.
[12] Wang X, Wang W, Li L, Perry G, Lee HG, Zhu X. Oxidative stress and mitochondrial dysfunction in Alzheimer's disease. Biochim Biophys Acta 2014;1842(8):1240–7.
[13] Hauptmann S, Scherping I, Dröse S, Brandt U, Schulz KL, Jendrach M, et al. Mitochondrial dysfunction: an early event in Alzheimer pathology accumulates with age in AD transgenic mice. Neurobiol Aging 2009;30(10):1574–86.
[14] Leuner K, Schütt T, Kurz C, Eckert SH, Schiller C, Occhipinti A, et al. Mitochondrion-derived reactive oxygen species lead to enhanced amyloid beta formation. Antioxidants Redox Signal 2012;16(12):1421–33.
[15] Wang X, Su B, Lee HG, Li X, Perry G, Smith MA, et al. Impaired balance of mitochondrial fission and fusion in Alzheimer's disease. J Neurosci 2009;29(28):9090–103.
[16] Manczak M, Calkins MJ, Reddy PH. Impaired mitochondrial dynamics and abnormal interaction of amyloid beta with mitochondrial protein Drp1 in neurons from patients with Alzheimer's disease: implications for neuronal damage. Hum Mol Genet 2011;20(13):2495–509.
[17] Lunnon K, Keohane A, Pidsley R, Newhouse S, Riddoch-Contreras J, Thubron EB, et al. Mitochondrial genes are altered in blood early in Alzheimer's disease. Neurobiol Aging 2017;53:36–47.
[18] Huang Q, Zhan L, Cao H, Li J, Lyu Y, Guo X, et al. Increased mitochondrial fission promotes autophagy and hepatocellular carcinoma cell survival through the ROS-modulated coordinated regulation of the NFKB and TP53 pathways. Autophagy 2016;12(6):999–1014.
[19] Fang EF, Hou Y, Palikaras K, Adriaanse BA, Kerr JS, Yang B, et al. Mitophagy inhibits amyloid-β and tau pathology and reverses cognitive deficits in models of Alzheimer's disease. Nat Neurosci 2019;22(3):401–12.
[20] Macdonald R, Barnes K, Hastings C, Mortiboys H. Mitochondrial abnormalities in Parkinson's disease and Alzheimer's disease: can mitochondria be targeted therapeutically? Biochem Soc Trans 2018;46(4):891–909.
[21] Grimm A, Eckert A. Brain aging and neurodegeneration: from a mitochondrial point of view. J Neurochem 2017;143(4):418–31.
[22] Feng S, Wan S, Liu S, Wang W, Tang M, Bai L, et al. LARS2 regulates apoptosis via ROS-mediated mitochondrial dysfunction and endoplasmic reticulum stress in ovarian granulosa cells. Oxid Med Cell Longev 2022;2022:5501346.
[23] Zhou W, Feng X, Li H, Wang L, Zhu B, Liu W, et al. Inactivation of LARS2, located at the commonly deleted region 3p21.3, by both epigenetic and genetic mechanisms in nasopharyngeal carcinoma. Acta Biochim Biophys Sin 2009;41(1):54–62.
[24] Feng S, Wan S, Liu S, Wang W, Tang M, Bai L, et al. LARS2 regulates apoptosis via ROS-mediated mitochondrial dysfunction and endoplasmic reticulum stress in ovarian granulosa cells. Oxid Med Cell Longev 2022;2022:1–18.
[25] Capriglia F, Rizzo F, Petrosillo G, Morea V, d'Amati G, Cantatore P, et al. Exploring the ability of LARS2 carboxy-terminal domain in rescuing the MELAS phenotype. Life 2021;11(7).
[26] Riley LG, Rudinger-Thirion J, Schmitz-Abe K, Thorburn DR, Davis RL, Teo J, et al. LARS2 variants associated with hydrops, lactic acidosis, sideroblastic anemia, and multisystem failure. JIMD Rep 2016;28:49–57.
[27] van der Knaap MS, Bugiani M, Mendes MI, Riley LG, Smith DEC, Rudinger-Thirion J, et al. Biallelic variants in LARS2 and KARS cause deafness and (ovario) leukodystrophy. Neurology 2019;92(11):e1225–37.
[28] Wang Z, Lu Z, Lin S, Xia J, Zhong Z, Xie Z, et al. Leucine-tRNA-synthetase-2-expressing B cells contribute to colorectal cancer immunoevasion. Immunity 2022;55(6). 1067-81.e8.
[29] Reddrop C, Moldrich RX, Beart PM, Farso M, Liberatore GT, Howells DW, et al. Vampire bat salivary plasminogen activator (desmoteplase) inhibits tissue-type plasminogen activator-induced potentiation of excitotoxic injury. Stroke 2005;36(6):1241–6.
[30] Samson AL, Nevin ST, Croucher D, Niego B, Daniel PB, Weiss TW, et al. Tissue-type plasminogen activator requires a co-receptor to enhance NMDA receptor function. J Neurochem 2008;107(4):1091–101.

[31] Li L, Jiang Y, Wu G, Mahaman YAR, Ke D, Wang Q, et al. Phosphorylation of truncated tau promotes abnormal native tau pathology and neurodegeneration. Mol Neurobiol 2022;59(10):6183–99.
[32] Neyroud AS, Rudinger-Thirion J, Frugier M, Riley LG, Bidet M, Akloul L, et al. LARS2 variants can present as premature ovarian insufficiency in the absence of overt hearing loss. Eur J Hum Genet 2023;31(4):453–60.
[33] Kiss H, Kedra D, Yang Y, Kost-Alimova M, Kiss C, O'Brien KP, et al. A novel gene containing LIM domains (LIMD1) is located within the common eliminated region 1 (C3CER1) in 3p21.3. Hum Genet 1999;105(6):552–9.
[34] Riley LG, Rudinger-Thirion J, Frugier M, Wilson M, Luig M, Alahakoon TI, et al. The expanding LARS2 phenotypic spectrum: HLASA, Perrault syndrome with leukodystrophy, and mitochondrial myopathy. Hum Mutat 2020;41(8):1425–34.
[35] González-Serrano LE, Chihade JW, Sissler M. When a common biological role does not imply common disease outcomes: disparate pathology linked to human mitochondrial aminoacyl-tRNA synthetases. J Biol Chem 2019;294(14):5309–20.
[36] Rubio Gomez MA, Ibba M. Aminoacyl-tRNA synthetases. RNA 2020;26(8):910–36.
[37] Chen J, Liu W. Lin28a induced mitochondrial dysfunction in human granulosa cells via suppressing LARS2 expression. Cell Signal 2023;103:110536.
[38] Blass JP, Baker AC, Ko L, Black RS. Induction of Alzheimer antigens by an uncoupler of oxidative phosphorylation. Arch Neurol 1990;47(8):864–9.
[39] Szabados T, Dul C, Majtényi K, Hargitai J, Pénzes Z, Urbanics R. A chronic Alzheimer's model evoked by mitochondrial poison sodium azide for pharmacological investigations. Behav Brain Res 2004;154(1):31–40.
[40] Swerdlow RH, Burns JM, Khan SM. The Alzheimer's disease mitochondrial cascade hypothesis: progress and perspectives. Biochim Biophys Acta 2014;1842(8):1219–31.
[41] Andrade-Guerrero J, Santiago-Balmaseda A, Jeronimo-Aguilar P, Vargas-Rodríguez I, Cadena-Suárez AR, Sánchez-Garibay C, et al. Alzheimer's disease: an updated overview of its genetics. Int J Mol Sci 2023;24(4).
[42] Martin SA, Souder DC, Miller KN, Clark JP, Sagar AK, Eliceiri KW, et al. GSK3β regulates brain energy metabolism. Cell Rep 2018;23(7). 1922-31.e4.
[43] DaRocha-Souto B, Coma M, Pérez-Nievas BG, Scotton TC, Siao M, Sánchez-Ferrer P, et al. Activation of glycogen synthase kinase-3 beta mediates β-amyloid induced neuritic damage in Alzheimer's disease. Neurobiol Dis 2012;45(1):425–37.
[44] Serenó L, Coma M, Rodríguez M, Sánchez-Ferrer P, Sánchez MB, Gich I, et al. A novel GSK-3beta inhibitor reduces Alzheimer's pathology and rescues neuronal loss in vivo. Neurobiol Dis 2009;35(3):359–67.
[45] Chauhan N, Paliwal S, Jain S, Verma K, Paliwal S, Sharma S. GSK-3β and its inhibitors in Alzheimer's disease: a recent update. Mini Rev Med Chem 2022;22(22):2881–95.
[46] Jere SW, Houreld NN, Abrahamse H. Role of the PI3K/AKT (mTOR and GSK3β) signalling pathway and photobiomodulation in diabetic wound healing. Cytokine Growth Factor Rev 2019;50:52–9.
[47] Gao YL, Liu CS, Zhao R, Wang LL, Li SS, Liu M, et al. [Effects of PI3K/akt pathway in wound healing process of mice skin]. Fa Yi Xue Za Zhi 2016;32(1):7–12.
[48] Peng M, Ling X, Song R, Gao X, Liang Z, Fang F, et al. Upregulation of GLT-1 via PI3K/Akt pathway contributes to neuroprotection induced by dexmedetomidine. Front Neurol 2019;10:1041.
[49] Liu S, Xu L, Shen Y, Wang L, Lai X, Hu H. Qingxin Kaiqiao Fang decreases Tau hyperphosphorylation in Alzheimer's disease via the PI3K/Akt/GSK3β pathway in vitro and in vivo. J Ethnopharmacol 2024;318(Pt B):117031.
[50] Kma L, Baruah TJ. The interplay of ROS and the PI3K/Akt pathway in autophagy regulation. Biotechnol Appl Biochem 2022;69(1):248–64.
[51] Zhang J, Wang X, Vikash V, Ye Q, Wu D, Liu Y, et al. ROS and ROS-mediated cellular signaling. Oxid Med Cell Longev 2016;2016:4350965.
[52] Leslie NR, Downes CP. PTEN: the down side of PI 3-kinase signalling. Cell Signal 2002;14(4):285–95.